Basic Electrochemical Performance of Pure LiMnPO$_4$: a Comparison with Selected Conventional Insertion Materials

Jože Moškon, Maja Pivko and Miran Gaberšček*

National Institute of Chemistry, Ljubljana, Slovenia, Hajdrihova 19, SI-1000 Ljubljana

* *Corresponding author: E-mail: miran.gaberscek@ki.si*
Phone: +386 1 4760 320

This paper is dedicated to Prof. Janko Jamnik, our unforgettable coworker, leader and friend.

Abstract

We compare the basic electrochemical performance of a LiMnPO$_4$ battery material with the performance of its much more researched olivine counterpart – LiFePO$_4$. To get a wider picture, we also included another well understood material, LiCoO$_2$. Based on chronopotentiometric (galvanostatic) experiments, we discuss the materials performance in terms of cell energy efficiency and electrode polarization. We propose and justify the use of the "inflection point criterion" for determination of total overpotential (η_{total}). We further demonstrate that the general current-overpotential characteristics can be represented by introducing the total resistance of the cell – R_{total}. We find consistently that whereas in LCO the general current-overpotential characteristics is more or less linear, there is significant deviation from linearity in LiFePO$_4$ and even bigger in LiMnPO$_4$. The phenomenon is discussed in terms of state-of-the art knowledge about phase transformation phenomena in these materials.

Keywords: Insertion battery materials, LiMnPO$_4$, non-linearity, activation, efficiency, kinetics

1. Introduction

Soon after their invention, significant differences in the electrochemical performance of different members of the phospho-olivine polyanionic family LiMPO$_4$ (M = Fe, Mn, Co, Ni) were observed. For example, it was assumed that the iron analogue, LiFePO$_4$ (LFP), was exhibiting good enough electrochemical performance to be considered as potentially interesting material for low-power battery applications.[1] By contrast, from the manganese analogue, LiMnPO$_4$ (LMP), basically no lithium could be extracted, neither electrochemically nor chemically.[1] Similar dichotomy persisted for many years, with LMP being able to deliver only a fraction of the reversible theoretical capacity – at low C-rates and with a big potential difference between the charge and discharge curves.[2–4] After demonstration of much improved performance when used in mixtures with LFP,[5,6] the interest in this material has grown considerably. In parallel to that, improvements of the performance of pure LMP have also been occasionally

reported. For instance, in 2002 Sony published a reversible capacity of 140 mAh/g for LMP at room temperature (CC-CV cycling protocol with potential window 2.0–4.5 V),[7] but this achievement could then not be reproduced for many years.

An obvious approach to improving the rate performance of insertion materials seems to be decreasing the particle size.[8] Drezen et al.[9] were the first to demonstrate the beneficial effect of particle size minimization on the electrochemistry of LMP. In particular, they used a polyol synthesis approach to prepare nanoparticles of LMP material with a platelet morphology. Particles having a thickness of about 30 nm were subsequently carbon coated in a ballmilling step. A version of this procedure yielded spherical LMP particles with a quite uniform particle size of 25–30 nm coated with relatively thick (~15 nm) carbon layer delivering 145 mAhg^{-1} at C/20 and giving a stable reversible capacity of 140 mAhg^{-1} for C/10 C-rate (both at 30 °C using a CC-CV cycling protocol).[10,11] Oh et al.[12] reported a synthesis of carbon–LiMnPO$_4$ nanocomposite by

ultrasonic spray pyrolysis followed by ballmilling with carbon. In the case of a LiMnPO$_4$-C material having a native carbon content of ~27 wt.% and 7.5 wt.% of additional carbon black they obtained a reversible capacity of 158 mAhg^{-1} at C/20 (at 25 °C using a CC-CV cycling protocol). Choi et al.[13] synthesized LiMnPO$_4$ nanoplates *via a* solid-state reaction in molten hydrocarbon. After ball milling with 20 wt.% of conductive carbon, the LMP-based cathode material demonstrated high and stable specific capacity – exceeding 150 mAh/g in initial C/25 cycles and retained ~145 mAh/g after pro-longed cycling (CC protocol in voltage range 2.0–4.5 V). Later on, Kang et al.[14] reported that small amounts of Fe and Mg dopants significantly improved the electrochemical power performance of LiMnPO$_4$. Rangappa et al.[15] prepared monodisperse nanoparticles of LiMnPO$_4$ by performing synthesis under supercritical fluid conditions and reported the electrochemical performance of subsequently carbon coated 20 nm sized LMP to be 156 mAh/g (at C/100 and the lower cut off voltage 2 V).

More recently,[16] we introduced a two-step synthesis method which yielded LMP with a primary particle size around ~20–50 nm. In order to keep individual particles sufficiently separated but still in electronic contact we embedded them into pyrolytic carbon, an approach known from many other studies on various insertion materials.[17–27] Our material delivers an initial reversible capacity of ~160 mAhg^{-1} at a C-rate of C/20 at 55 °C using a CC cycling protocol and ~155 mAhg^{-1} for C/20 C-rate at 25 °C using a CC-CV cycling protocol.

Despite the great advances described above, the practical performance of LMP still lags significantly behind that of LFP. In order to understand the critical differences between the two materials, we have performed several systematic sets of experiments on both materials and also on some other well understood insertion materials, such as LiCoO$_2$. The most important similarities and differences are shown and discussed in some detail. Quite surprisingly we find that, in fact, the properties of LMP are not essentially different from those of LFP, only the relaxation of charge within the lattice of Li$_x$MnPO$_4$ is significantly slower. This, however, implies that if very small particles of LMP (according to our estimation on the order of 10 nm) could be efficiently wired both ionically and electronically, there should be no obstacles for this material to reach its theoretical limitation of capacity, 171 mAh/g, and a high C-rate capability.

2. Experimental

2. 1. Active Materials

LiCoO$_2$-based cells were prepared using a commercial LiCoO$_2$ ("cathode powder SC 20", Merck) with an average particle size of 2–3 μm. LiFePO$_4$-C active material was synthesized according to a citrate precursor

method described in detail elsewhere.[28] Briefly, Fe(III) citrate (Aldrich) was dissolved in water at 60 °C. Separately, an equimolar aqueous solution of LiH$_2$PO$_4$ was prepared from H$_3$PO$_4$ (Merck) and Li$_3$PO$_4$ (Aldrich). The solutions were mixed together and after 1 h of stirring a rotary evaporator was used for the removal of water (at 60 °C under reduced pressure). After thorough drying and subsequent grinding with a mortar and pestle, the obtained greenish xerogel was fired in argon atmosphere for 10 h at 700 °C. The heating rate was 10 °C/min. This method gives porous LiFePO$_4$ particles of typical sizes between 5 and 20 μm. All particle surfaces (outer and inner) were essentially covered with a 1–2 nm thick carbon film. The total content of native amorphous carbon was ~ 3 wt%. The LiMnPO$_4$-C (LMP) active material was synthesized according to the two-step synthesis described in detail elsewhere.[16] In the first step, a homogeneous mixture of reactants without lithium was prepared in a round bottom flask by stirring stoichiometric quantities of manganese acetate (Fluka), citric acid (Sigma-Aldrich), and phosphoric acid (Merck) (the molar ratio of Mn:P:citric acid was 1:1.1:1.5). The pre-dissolved Mn and P precursors and solution of citric acid (each prepared as separate water solution) were mixed together at RT in a flask. The latter was then transferred to a vacuum rotary evaporator with a bath temperature of 60 °C. In the first step of drying the pressure was carefully decreased to 60 mbar whereby most of the water was removed forming a viscous sol that was subjected to a sudden pressure decrease to 10 mbar whereby the sol simultaneously expanded to form a voluminous foamy-like sol that was finally dried at 5 mbar for 2 h. The dried sol was thermally treated at 700 °C for 1 h in an argon atmosphere. In the second step, the composite from the first step was mixed with a 20% excess of LiOH (Aldrich, the molar ratio Li:Mn = 1.2:1), using planetary ball milling (Retch) for 30 min at 300 rpm. The final LiMnPO$_4$-C material was obtained with additional thermal treatment at 700 °C in argon for 12 h.

2. 2. Preparation of Electrode Composites and Electrodes

Cathode composites were prepared from the basic active materials (LiCoO$_2$, LiFePO$_4$-C, LiMnPO$_4$-C) to which carbon black (CB, "Printex") and binder (PTFE) were added to get a final weight ratio of 8:1:1. A mixture consisting from active material, CB and 60% PTFE (Aldrich) in 2-propanol was prepared. The mixture was homogenized by thoroughly mixing in a ball mill (30 min at 300 rpm). After evaporation of the 2-propanol a ductile kneadable composite mass was obtained. The electrodes were prepared by spreading the cathode composite mass onto an aluminum foil current collector that had been roughened using a sandpaper to improve clinging. Circular electrodes with a diameter of 14 mm (1.54

cm^2) were cut out. The electrodes were pressed with a force of 5 tons for 1 min in a hydraulic press. The typical loading of active material in electrodes was 3–3.5 mg/cm^2. Finally, the electrodes were dried for 12 h at 90 °C and stored in an Ar filled glovebox for at least 24 h before use.

2. 3. Cell Preparation and Electrochemical Measurements

The electrochemical characteristics were measured in vacuum-sealed cells ("pouch cells"). Two electrode cells were assembled: the tested working electrode (WE) and a metallic Li counter electrode (CE) (~3 cm^2) were placed oppositely over a separator ("Whatman" glass microfiber). The electrolyte used was 1 M LiPF$_6$ in EC:DEC (1:1 by volume), all received from Aldrich. The galvanostatic measurements were performed using a "VMP3" (Bio-Logic) potentiostat/galvanostat running with EC-Lab® software. All the comparative measurements of LiCoO$_2$, LiFePO$_4$-C, LiMnPO$_4$-C materials were conducted at 25 °C.

3. Results and Discussion

The structure and morphology of LMP prepared *via* the two-step synthesis developed in our laboratory were reported previously.[16] Also, degradation processes appearing during various stages of cycling were recently thoroughly examined using a range of techniques.[29] Briefly, all diffraction peaks correspond to the olivine type structure with a *Pnma* space group of the orthorhombic crystal system. The Rietveld refinement showed, however, that our LMP had a slightly smaller cell volume – the difference being in the range ~0.1–0.6% compared to the previously reported data if compared to LiMnPO$_4$ samples obtained in earlier studies,[10,12,13,30–32] or to our reference sample with bigger crystallites. This deviation still needs to be explained. The estimated particle size from peak broadening is (38 ± 2) nm which matches well with the observation using SEM and TEM.[16] LiMnPO$_4$ particles are very well dispersed in carbon matrix (14 wt.% of C in LiMnPO$_4$-C) formed during the first step of the synthesis. The small, well separated but electronically wired particles resulted in very good electrochemistry: a capacity up to 161.5 mAh/g or 94% of the theoretical value (171 mAh/g).

The LFP active material synthesized according to a citrate precursor method[28] appears as porous LiFePO$_4$-C secondary particles of typical sizes between 5 and 20 μm, whereby all particle's surfaces (outer and inner) are essentially covered with an average 1–2 nm thick carbon film.[4] The structure and morphology of LFP prepared by this synthesis developed in our laboratory were reported previously.[4,28] Briefly, all diffraction peaks correspond to the

olivine type structure with a *Pnma* space group of the orthorhombic crystal system. The Rietveld refinement shows, similar to the LMP material, that our LFP with unit cell volume of 290.58 Å^3 has a slightly smaller cell volume – on the order of ~0.3% – compared to the experimentally obtained[33] and generally accepted value of 291.4 Å^3.[34] This deviation could be related to nano-sizing. Unfortunately, a more detailed analysis is rather difficult as the exact primary particle size is difficult to determine for such a porous type of particles.

Although high specific capacities using LMP electrodes have been obtained, several other important electrochemical features have remained poorly understood. Examples of such features are: low power density (rapid decay of capacity above 1C), unusually large voltage hysteresis (~ 200 mV) between charge and discharge curve already at relatively low rates (C/20) and asymmetry of charge-discharge curve. These issues are systematically addressed in the present paper.

3. 1. Galvanostatic Measurements: Voltage Hysteresis and Energy Efficiency (ε)

Fig. 1a shows measured galvanostatic charge-discharge curves for LMP at different C-rates in the range from C/20 up to 16C at 25 °C. The potential window was 2.7–4.5 V vs. Li using the conventional constant-current "CC" cycling protocol. A comparison to the well-known LFP (Fig. 1b) and LCO (Fig. 1c) electrodes tested under similar conditions shows one particular difference: in LFP and LCO the voltage hysteresis between charge and discharge at low rates is rather small (34 mV and 14 mV for LFP and LCO, respectively, at C/10) but then significantly increases when progressing to higher rates (for example approaching to 400 mV at 5C). By contrast, in LMP the voltage hysteresis is quite large (~ 200 mV) already at smallest cycling rate (C/20) but then surprisingly remains within tolerable range as the rate increases (eg. ca 550 mV at 4C). Note that all the cells had the same geometric surface area of the electrode (1.5 cm^2), the same electrode composition (80 wt.% active material, 10 wt.% carbon black ("Printex") and 10 wt.% of PTFE binder) and were prepared using the same procedure (1 min of pressing with force of 5 tons in a hydraulic press). The active mass loadings of the electrodes were comparable: 4.3 mg in the case of LiMnPO$_4$, 5.2 mg in the case of LiFePO$_4$, and 4.1 mg in the case of LiCoO$_2$ based electrode.

The unexpectedly good behaviour of LMP at higher rates is even more clearly seen from Figs. 2 (a)–2 (c) which show a comparison of selected galvanostatic cycles at similar current densities that are presented in terms of the mass-normalized current I_m (in A per g of active material). The voltage hysteresis of LMP at low rates is distinctly larger than in the case of LFP and LCO. However, with increasing rate, especially above ca. 1C (Fig.
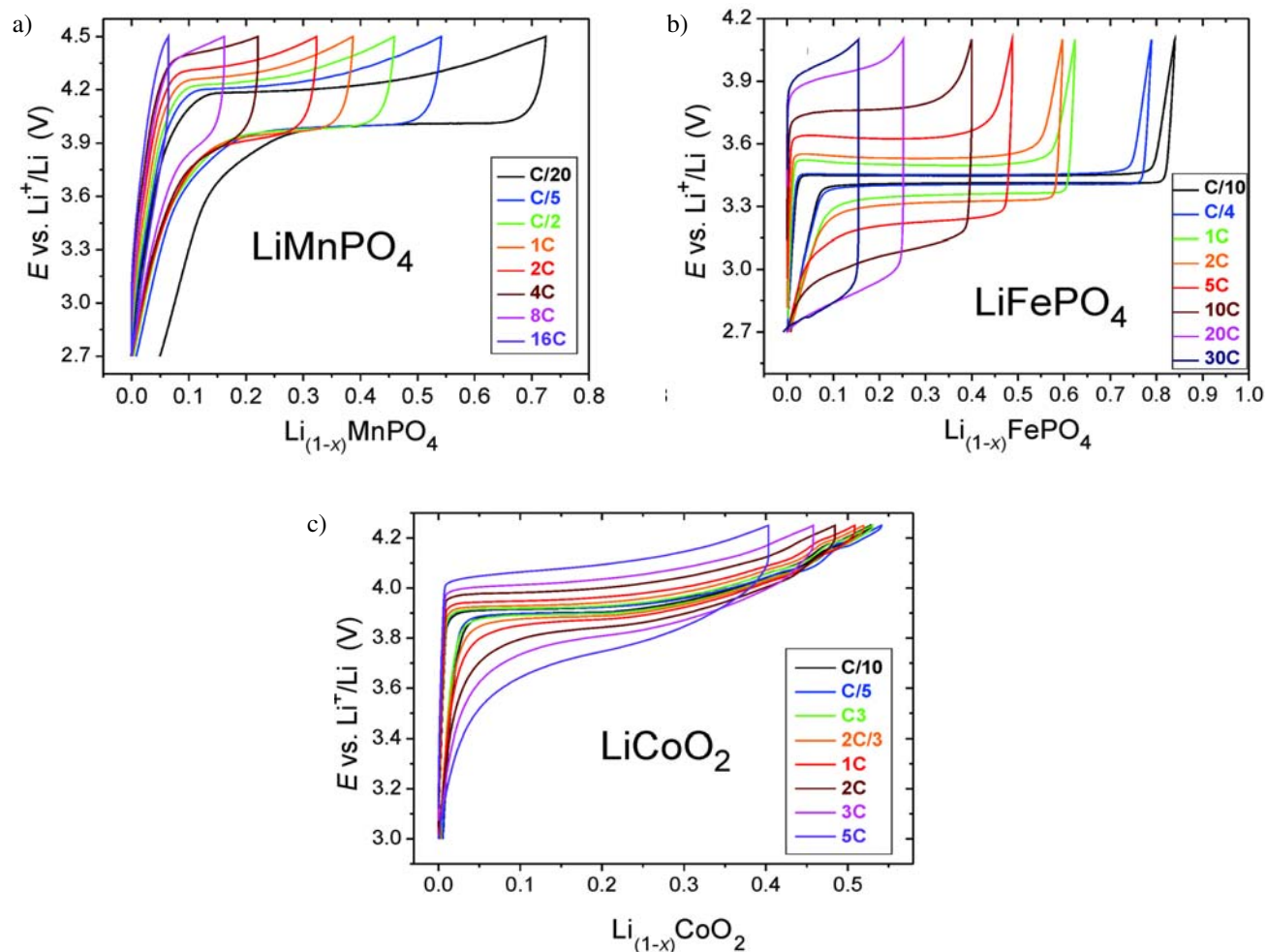
Figure 1. Comparison of a series of galvanostatic cycles measured on different cells at different current densities: a) LiMnPO$_4$ (from C/20 up to 16C in the potential window 2.7–4.5 V vs. Li), b) LiFePO$_4$ (from C/10 up to 30C in the potential window 2.7–4.1 V vs. Li) and c) LiCoO$_2$ (from C/10 up to 5C in the potential window 3.0–4.25 V vs. Li). In all the cases the third cycle measured at certain C-rate is plotted; all the curves were measured at 25 °C and obtained using the conventional constant-current "CC" cycling protocol.

2c), the hysteresis of LMP becomes comparable to the hysteresis for LFP and LCO – which is rather unexpected. Without trying to find a deeper mechanistic reason, we here mainly comment this result in terms of energy efficiency of the various cells, ε. The latter can be defined as follows:

$$\varepsilon = \frac{-\Delta W(\text{discharge})}{\Delta W(\text{charge})} \quad (1),$$

where $\Delta W(\text{charge})$ and $\Delta W(\text{discharge})$ are the total energy changes in the cell during galvanostatic charge and discharge. The total energy that is transferred to/from an electrochemical cell is assumed to be equal to the change of the electrical energy of the cell, ΔW, and is obtained simply by integration:

$$W_{e,2} - W_{e,1} = \Delta W_e = I \int_{t1}^{t2} V(t)dt \quad (2),$$

where indexes 1 and 2 correspond to the start and end of charge (or discharge) process, I is the constant current and $V(t)$ the measured voltage of the cell during charge (or discharge) as a function of time, t. The obtained energy efficiencies (ε) of the cells for sets of measured galvanostatic curves shown on Fig. 1 are shown on Fig. 2d where there are plotted versus normalized current, I_m.

It is generally expected for battery systems that the energy efficiency be reduced when increasing the current density. The results of Fig. 2d are in line with this hypothesis, except in the case of LMP at the lowest tested rate (C/20) where unexpectedly low efficiency (85%) was obtained. This deviation is due to the large coulombic irreversibility of the C/20 galvanostatic cycle (see Fig. 1a), that was measured as the third C/20 cycle in a sequence starting with the "pristine electrode" with the LiMnPO$_4$-C material in the pristine state. As shown in our recent paper,[29] LMP electrodes exhibit a strong irreversibility due to different types of parasitic side reactions that are taking

place during charge at high potentials (especially in the initial cycles).[11,35] In any case, we may conclude that at low current densities the energy efficiency, ε, of LMP is substantially smaller than in the other two active materials, LFP and LCO.

At C/5 rate the LMP based cell has the energy efficiency of 90%, still being much smaller than that of the LCO (98% at C/5) and LFP (97% at C/10) based cells. With increasing current the efficiency of LCO gradually becomes distinctly higher compared to the efficiency of the other two olivine materials. However, there are also pronounced differences in the behaviour of LMP and LFP: quite surprisingly, the rate of efficiency decrease is smaller in the case of LMP, so increasing the current density sufficiently (e.g. above ~ 1.5 A/g), ε of LMP becomes even higher than that of LPF.

Based on Fig. 2d one could come to a conclusion that in some aspects LiMnPO$_4$ exhibits a better electrochemistry performance than LiFePO$_4$. This however would

be in contradiction with the known data for conductivity of the two materials at RT,[3,36] as well as with the experimental data for the lithium diffusion coefficient in these two materials. Specifically, for LFP and LMP the experimentally determined diffusion coefficients for Li range from ~10^{-13} to ~10^{-16} cm^{2}s^{-1} and 10^{-16} to 10^{-17} cm^{2}s^{-1}, respectively.[22,37–40]

A deeper analysis shows that plots such as that in Fig. 2d need to be interpreted with additional care taking into account various limitations of such an approach. For example, one finds that, at high rates, the energy efficiency obtained using Eq. (1) is strongly affected by the fact that at these conditions the active material cannot be fully charged and discharged. In our specific case this means that the measured average voltage of the cell during charge is artificially reduced and the average voltage during discharge is artificially increased. Consequently, at high C-rates the calculated energy efficiencies using Eq. (1) are overestimated. Conversely, for the low and me-
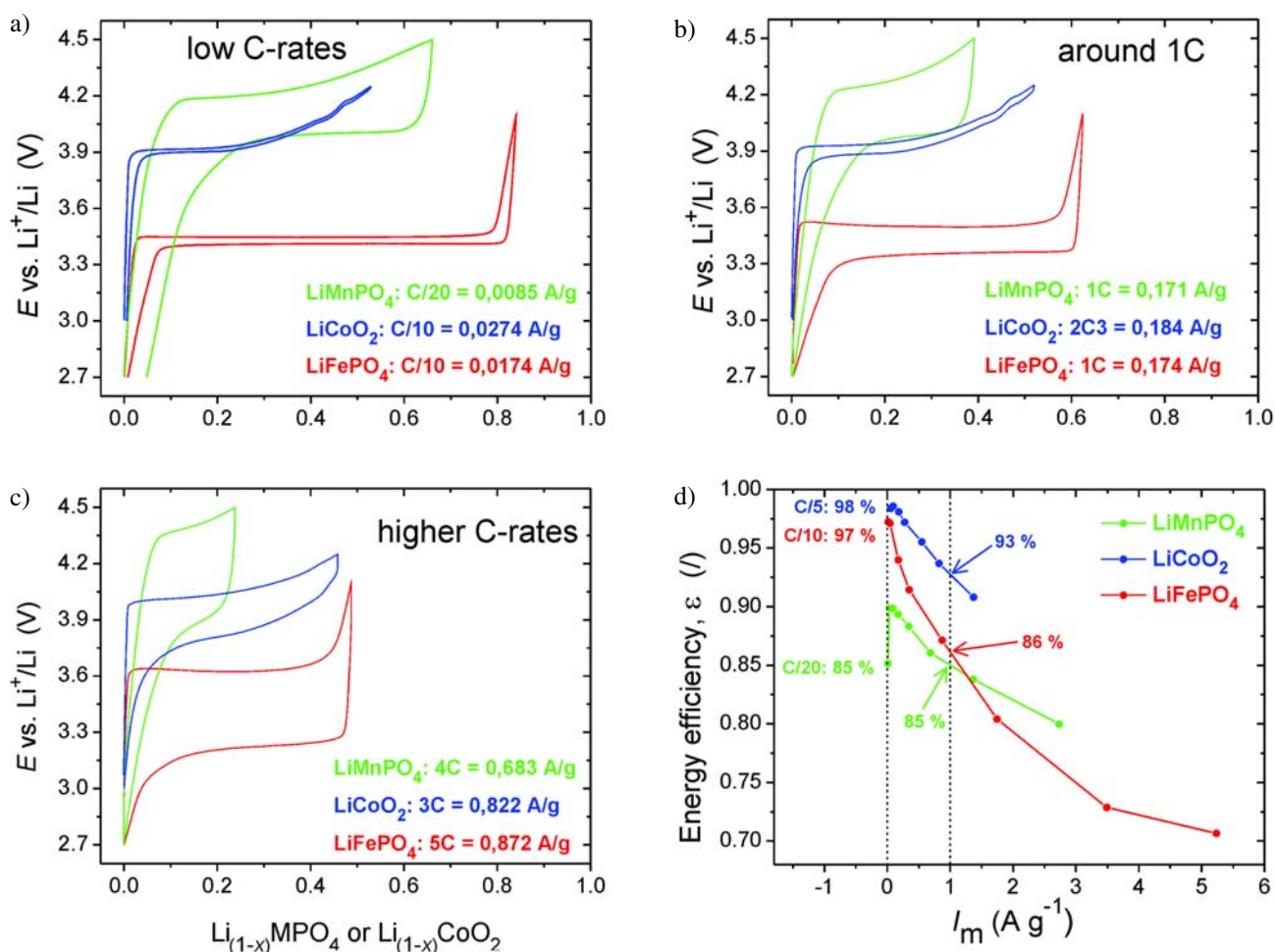

Figure 2. Direct comparison of the shape of selected galvanostatic cycles measured on LiFePO$_4$ (red line), LiCoO$_2$ (blue line) and LiMnPO$_4$ (green line) based electrodes at: a) low, b) medium, and c) higher current densities. The current densities shown are presented in terms of the normalized current, I_m. In all the cases the third cycle at the same C-rate is plotted. d) Energy efficiencies (ε) of the cells calculated using Equation (1) and plotted versus normalized current, I_m.

dium C-rates where still a substantial part of total capacity (e.g. > 1/3 of theoretical capacity) is exploited the obtained values of ε are meaningful. Thus in the case of the LMP at 4C, 8C and 16 C (Fig. 1a) and in the case of the LFP at 20C and 30C (Fig. 1b) the obtained values of ε are larger than the real ones (those with the true physical meaning). More realistic values of ε for high C-rates could be obtained by using a wider potential window which, however, would only be possible with a much improved electrolyte that would exhibit excellent ion transport properties together with possessing much wider potential stability window compared to the presently used carbonate-based electrolytes.

3. 2. Current-Overpotential (I-η) Characteristics

In an attempt to gain a more realistic insight into inherent electrochemical performance at different rates we have made additional analyses of the hysteretic behavior of the three materials discussed above. As the hysteresis between the charge and discharge curve varies significantly with the state of charge/discharge (SOC/SOD) (see Figs. 2a–c), an obvious question arises: at which points in the charge and discharge curve should we read out the value of overpotential, η? One possibility would be to decide for a fixed value of SOC/SOD (e.g. reading the potential at fixed Δx in $Li_{(1-x)}MnPO_4$). We have found that choosing, for example $\Delta x = 0.1$, could be quite a good criterion in the case of LFP which exhibits very pronounced potential plateau. However, this criterion is less appropriate for the case of discharge of LCO and for the charge of LMP at lower rates (e.g. C/20) where we do not reach the plateau region yet.

Fig. 3 shows a typical pair of galvanostatic curves of LFP measured at the same current (10C charge/10D discharge) and plotted as a function of time. We can easily observe 3 common regions: I) an initial steep increase/decrease in potential followed by a smooth transition into II) a plateau region with a distinctly "flat" voltage profile that expands into transition to III) a steeper "blocking-like" ending of the galvanostatic curve with progressively increasing/decreasing slope. In LFP all the 3 regions are well expressed both for charge and discharge (see Fig. 1b); in the cases of LMP and LCO region III is not observed in the charge curves due to the fact that either the upper cut-off voltage simply chops away that portion of the curve (as in the case of LMP, see Fig. 1a) or the 2-phase plateau region is further followed by an additional charge-storage mechanism(s) which is/are reflected as additional features complicating the potential profile (as the subsequent transition to a single phase storage and followed by a phase transformation from hexagonal to monoclinic symmetry in the case of LCO,[41] see Fig. 1c).

We can further notice, however, that both curves shown in Fig. 3 have an inflection point (marked with red

dot) that is positioned inside region II. In a galvanostatic curve an inflection point has a physical meaning. Indirectly this is often recognized when authors choose to plot the first derivative of a galvanostatic curve as a function of potential. Generally, the first derivative, dE/dt, at a certain time t from the beginning of the charge/discharge corresponds to the reciprocal of the differential chemical capacitance, $1/C_{chem}$, at time t. If so, one finds that in the case of galvanostatic curve the inflection point corresponds to the global maximum of differential chemical capacitance, C_{chem}. At this particular time, t_{infl}, the potential of cell, E, varies the least with time (or SOC, x). In this sense, this can be seen as a unique point in a discharge/charge curve so we decided to use it as a reference point for evaluation of voltage hysteresis of any material under consideration.
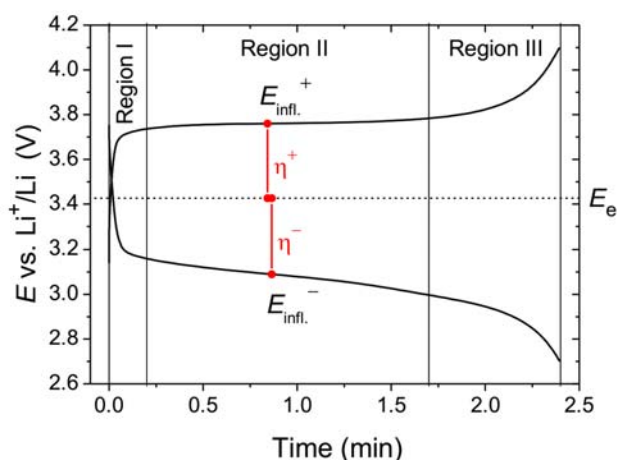
Figure 3. The inflection point criterion for determination of the value of the total overpotential (η_{total}) demonstrated on a typical pair of galvanostatic curves for LFP plotted as a function of time. The charge and discharge rates were the same (10C/10D). The charge/discharge total overpotentials (η^+_{total} and η^-_{total}) were obtained using Eq. 3. Indicated are the three common regions of a LFP galvanostatic profile.

We further define the total overpotential of the cell, η_{total}, as the difference between the measured voltage of the cell at the inflection point, E_{infl}, and the global equilibrium potential, E_e:

$$\eta_{total} = E_{infl} - E_e \quad (3),$$

where for E_e we took the mean value of potential in a plateau region of a galvanostatic cycle measured at very low current densities. Specifically, for LFP and LMP we took the values of 3.427 V and 4.105 V, respectively, obtained from corresponding ±C/1000 measurements (see also below).[42] For LCO the selected value was 3.909 V obtained from ±C/200 galvanostatic measurements. In all three cases the measurements were conducted at 25 °C. In Fig. 3 the total overpotentials for the charge and discharge are
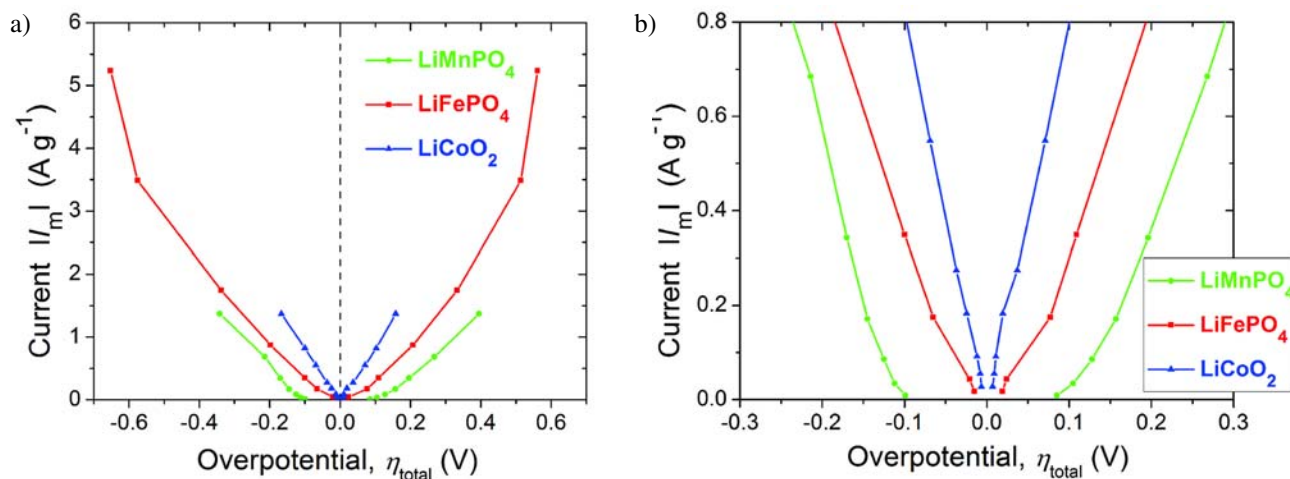
Figure 4. Current-Overpotential (I_m–η_{total}) characteristics of the compared LMP (green), LFP (red) and LCO (blue) obtained using the inflection point criterion together with Eq. 3. Data in panel (b) are merely a magnification of data in panel (a) for low current values. The data were extracted from the 3 sets of galvanostatic curves shown in Fig. 1.

denoted with "+" and "–" (η^+_{total} and η^-_{total}), respectively. It is worth noting that the proposed inflection point criterion for reading out the value of overpotential can be employed generally for different Li battery types including the one exhibiting the so called "solid solution" behaviour etc. The results of the analysis of the galvanostatic curves of the compared materials (LMP, LFP, LCO – Fig. 1) using the inflection point criterion are shown on Fig. 4. On the real axis the total overpotential (–η_{total}) is given in the positive (charge) and negative (discharge) direction. On the ordinate axis the normalized current (in A per g) is displayed.

Fig. 4 reveals that all 3 materials compared in this study exhibit quite symmetric I_m–η_{total} characteristics of increasing current with increased overpotential. We find that for all the measured current densities the overpotential (η_{total}) increases in the order: LCO LFP LMP. Further we can clearly see that LMP differs from the other two materials in having a much larger hysteresis at the lowest C-rate (close to 200 mV at C/20). A closer inspection of the results shows that the curves for LFP and LMP are bent forming a "U-shape". In other words – LFP and LMP based cells show a non-linear current-overpotential dependency. Performing further analyses (see below) in which we quantify the resistances of the measured cells, we show that such bending is an inherent property of LFP and LMP (and probably many other insertion materials).

One might argue that the appearance of the non-linear current-overpotential dependency could partly – or even entirely – be due to contribution of the electronic and/or ionic transport (wiring) within the electrode composites. Namely, it is well known that the measured electrochemical performance of Li ion insertion electrodes is strongly affected by the electrode morphology (electrode thickness, porosity and packing density) which has impact

on the course of overpotential curve and, consequently, on the obtained capacity. For the case of LFP based electrodes, this impact was systematically and thoroughly addressed by Lestriez et al.[43,44] and later effectively demonstrated in a major practical high-rate improvement of $Li_4Ti_5O_{12}$[45] and of LFP[46] based electrodes.

In the present specific case the effect of different wiring contribution could manifest itself through the higher density (approx. 5 g/cm^3) and larger particle size (micron) of $LiCoO_2$ compared for example to the nanosized and lower density (approx. 3.5 g/cm^3) LFP/LMP materials. This means that at the same electrode loading the $LiCoO_2$ electrode effectively appears (much) thinner than those of olivines. In order to check whether this difference in effective thickness and wiring has any effect on the current-overvoltage curve, we prepared a very thin LFP electrode (0.53 mg of $LiFePO_4$ per 1.54 cm^2). We measured its galvanostatic charge/discharge performance (supplementary Figure S1) using the same conditions as in the case of "standard" LFP electrode (5.2 mg per 1.54 cm^2) shown in Figure 1b. The current-overpotential (I_m–η_{total}) characteristics of the thin and standard LFP electrodes are compared in Figure 5.

As seen from Fig. 5, the current-overpotential characteristics of the "thin" LFP electrode expectedly exhibits comparatively smaller overpotential values across the whole current range (C/10–30C). However, also in the much thinner electrode the deviation from the linear (Ohm's law like) dependence is clearly detected. As in a (very) thin electrode the electronic and ionic "wiring" contributions are significantly reduced, if not vanishingly small, the persistent observation of non-linear dependence suggests that, at least in the olivines, the origin of the phenomenon is most probably due to their intrinsic bulk properties or, alternatively, due to properties of olivine/electrolyte interface.
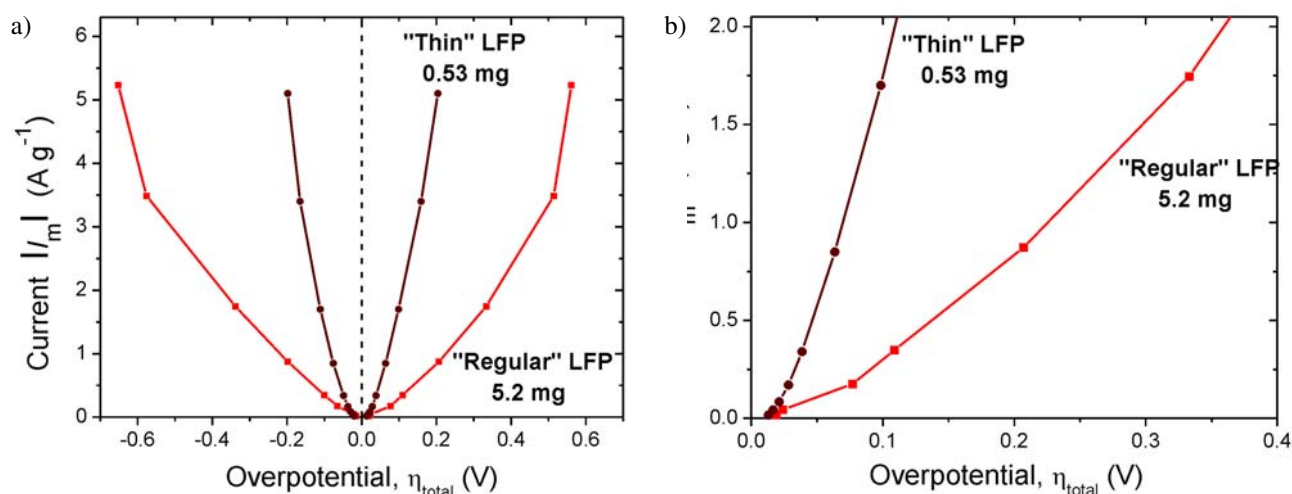
Figure 5. Absolute current-Overpotential (I_m–η_{total}) characteristics of the LFP electrode with "regular" thickness (5.2 mg, red, the same as in **Fig. 4**) and "thin" LFP electrode (0.53 mg, orange) obtained using the inflection point criterion together with Eq. 3. Data in panel (b) are merely a magnification of those in panel (a) for low and medium positive current values. The data for LFP with "regular" thickness was extracted from the set of galvanostatic curves shown in **Fig. 1b**, while for the "thin" LFP electrode from **Fig. S1**.

Aside from considering the potential wiring effect, one also needs to address the potential impact of the particle size and morphology of the different cathode materials (powders) used in this study. Namely, particle size can drastically influence the overpotential (and consequently capacity) during Li insertion/extraction, as well known from the very invention of LFP which was initially considered as an "…excellent candidate for the cathode of a low-power…".[1] Generally, one can roughly say that as we decrease the particle size from micron values towards 100 nm and less, the overvoltage consistently decreases at comparable currents.[47] Similarly active particle morphology and agglomeration of primary particles in secondary architecture definitely have an effect on the electrochemical performance. Particularly in particles of the two olivine materials with large aspect ratio (e.g. platelet morphology) the effects are strongly manifested due to the existence of preferential transport paths within the volume of the crystallites.

Despite the great impact of particle size and morphology on materials performance, we wish to emphasize once again that in the present work we do not focus on those, otherwise very important, issues but merely want to stress the **occurrence of a strong deviation of the current-overpotential characteristics from the linear dependence** which, to our knowledge, has not been sufficiently and convincingly treated in the literature. In other words, as regards Li ion batteries the data about the current-overpotential characteristics are quite rarely reported and the importance of the obtained results is even more rarely discussed. The aim of this manuscript is to open several directions along which some further progress towards understanding this phenomenon could be expected in the (near) future.

3. 3. Total Resistance of the Cell, R_{total}, and the "Activation" Phenomenon

We define the total resistance of the cell, R_{total}, as follows:

$$R_{\text{total}} = \frac{\eta_{\text{total}}}{I_{\text{meas}}}, \tag{4}$$

where I_{meas} is the measured value of current in galvanostatic experiment. Normalized total resistance of the cell, R_{total} m_{act}, is obtained simply by multiplying R_{total} with the mass of the active material in the electrode (m_{act}) and has the unit of Ωg.

The total resistances corresponding to the current-overpotential characteristics shown in Fig. 4 are presented in Fig. 6. For the cases of LMP- and LFP-based cells we can observe a very pronounced phenomenon: the total resistance of the cell decreases very much with the increasing current density (or, equivalently, C-rate). In the case of LFP-based electrode we briefly commented on this feature some time ago and termed it an "activation" phenomenon.[48] Later on, Lestriez et al.[43] performed a more systematic analysis of the measured galvanostatic curves of LFP electrodes and confirmed the existence of the phenomenon. They have also observed a similar non-linear characteristic for the case of nano-sized Si-based negative electrode.[49]

However, Fig. 6 also reveals that, in contrast to LMP and LFP, the resistance of the LCO-based electrode is relatively independent of the current density; in other words, the current-overpotential curve (see Fig. 4) is close to linear. One could say that, in a first approximation, the LCO-based cell is linear by nature and follows more or less the Ohm's law; when measured galvanostatically, a 10 fold increase of current (C-rate) will thus result in a
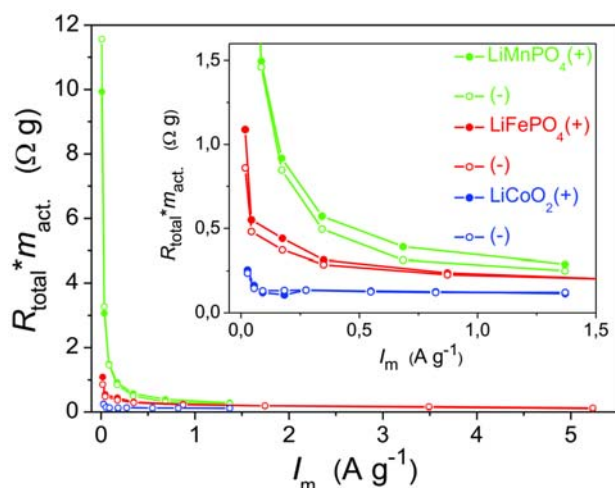
Figure 6. Total resistance of cell, R_{total}, for LMP- (green), LFP- (red) and LCO- (blue) based cells obtained using Eq. 4. The overpotential values were extracted using the inflection point criteria (see also data shown in Fig. 4). In order to compare different electrodes the resistances were mass-normalized $R_{total}m_{act}$, where m_{act} is the mass of active material. The obtained values of $R_{total}m_{act}$ for charge and discharge are denoted with (+) and (–), respectively.

10-fold increase of overpotential (or voltage hysteresis). In the case of LFP and LMP, however, there is a major deviation from Ohm's law: a 10 fold increase in current (C-rate) will result in much less than 10-fold overpotential increase. It seems that this electrode "activation" at higher rates is even more expressed for LMP.

The origin of electrode "activation" is still poorly understood. It might be correlated to the variable rate of the internal charge redistribution during charge/discharge at different rates,[50,51] but other options cannot be excluded. For example, it has been shown theoretically and confirmed experimentally that at very low currents active particles tend to phase-transform in a particle-by-particle fashion.[42,50,52–54] This means that a very small fraction of active material is in fact "active" at any given time during charge/discharge A more general simulation of porous insertion electrodes has suggested that the fraction of such "active" particles in the electrode scales with the current (charge/discharge rate).[55] Similarly it has been shown that imposing higher overpotentials during high current rate experiments induces more particles to undergo phase transformations at similar times during charge/discharge.[56,57] On the experimental level, extensive experimental observation of $LiFePO_4$ based electrodes using synchrotron Scanning Transmission X-Ray Microscopy (STXM) has confirmed that the fraction of the phase-transforming particles depends on C-rate.[51] It has been suggested that the electrode accommodates the higher current by increasing the active particle population.[51] Finally, *in-situ* XRD studies with high temporal resolution during high-rate galvanostatic cycling have revealed the formation of a nonequilibrium solid solution phase(s), Li_xFePO_4 ($0 < x < 1$),

where the distribution of solid solution compositions span the entire composition range between two thermodynamic phases, $LiFePO_4$ and $FePO_4$.[58,59] Thus, at high global current densities (e.g. 5C and higher) the fraction of the LFP electrode that reacts simultaneously via nonequilibrium solid solution increases with the increasing C-rate.[58,59]

In terms of the present results it is important to conclude that any of the mechanisms independently proposed in the above reports could be responsible for the observed current-voltage non-linearity ("activation" phenomenon). Namely, if we assume that the fraction of active particles indeed increases with C-rate (overpotential) then the results of Fig. 6 can be explained straightforwardly. Even more, in this case the curves shown in Fig. 6 could directly serve for estimation of the fraction of "active" particles at any given current (overpotential). Finally, if it is true that the current-voltage characteristic is non-linear due to increasing fraction of active particles, then certainly this is a new, previously unreported origin of current-voltage non-linearity in electrochemistry.

4. Conclusion

We discussed a couple of unusual phenomena in LMP and selected other insertion battery materials. For example, at current rates above ca. 1.5 A/g the energy efficiency of LMP, as calculated according to standard approaches, becomes even slightly higher than that of LFP and gradually approaches to that of LCO. We showed that this may be strongly correlated to the nature of overvoltage-current characteristic. Whereas in LCO this relationship is more or less linear, it deviates from linearity in both olivines. This non-linearity can be seen as an increasing activation of active material with increasing current rates. In LMP the activation is particularly strong which explains its good efficiency and the slowly increasing polarization at higher rates. One reason for the activation phenomenon in certain insertion materials could be the increase of fraction of particles that is actually undergoing phase transformation at given moment. If so, this is a different kind of non-linearity than typically observed in electrochemical systems (the non-linearity related to the well known Butler-Volmer equation). This hypothesis, however, still needs an experimental verification.

5. References

1. A. K. Padhi, K. S. Nanjundaswamy and J. B. Goodenough. *J. Electrochem. Soc.*, **1997**, *144*, 1188–1194.
2. C. Delacourt, P. Poizot, M. Morcrette, J.-M. Tarascon and C. Masquelier. *Chem. Mater.*, **2004**, *16*, 93–99.
3. C. Delacourt, L. Laffont, R. Bouchet, C. Wurm, J.-B. Leriche, M. Morcrette, J.-M. Tarascon and C. Masquelier. *J. Electrochem. Soc.*, **2005**, *152*, A913.

4. R. Dominko, M. Bele, M. Gaberscek, M. Remskar, D. Hanzel, J. M. Goupil, S. Pejovnik and J. Jamnik. *J. Power Sources*, **2006**, *153*, 274–280.

5. A. Yamada, M. Hosoya, S. C. Chung, Y. Kudo, K. Hinokuma, K. Y. Liu and Y. Nishi. *J. Power Sources*, **2003**, *119–121*, 232–238.

6. S. K. Martha, J. Grinblat, O. Haik, E. Zinigrad, T. Drezen, J. H. Miners, I. Exnar, A. Kay, B. Markovsky and D. Aurbach. *Angew. Chemie - Int. Ed.*, **2009**, *48*, 8559–8563.

7. G. Li, H. Azuma and M. Tohda. *Electrochem. Solid-State Lett.*, **2002**, *5*, A135.

8. M. Gaberscek, R. Dominko and J. Jamnik. *Electrochem. commun.*, **2007**, *9*, 2778–2783.

9. T. Drezen, N. H. Kwon, P. Bowen, I. Teerlinck, M. Isono and I. Exnar. *J. Power Sources*, **2007**, *174*, 949–953.

10. D. Wang, H. Buqa, M. Crouzet, G. Deghenghi, T. Drezen, I. Exnar, N. H. Kwon, J. H. Miners, L. Poletto and M. Grätzel. *J. Power Sources*, **2009**, *189*, 624–628.

11. S. K. Martha, B. Markovsky, J. Grinblat, Y. Gofer, O. Haik, E. Zinigrad, D. Aurbach, T. Drezen, D. Wang, G. Deghenghi and I. Exnar. *J. Electrochem. Soc.*, **2009**, *156*, A541.

12. S. M. Oh, S. W. Oh, C. S. Yoon, B. Scrosati, K. Amine and Y. K. Sun. *Adv. Funct. Mater.*, **2010**, *20*, 3260–3265.

13. D. Choi, D. Wang, I. T. Bae, J. Xiao, Z. Nie, W. Wang, V. V. Viswanathan, Y. J. Lee, J. G. Zhang, G. L. Graff, Z. Yang and J. Liu. *Nano Lett.*, **2010**, *10*, 2799–2805.

14. J. Kim, Y.-U. Park, D.-H. Seo, J. Kim, S.-W. Kim and K. Kang. *J. Electrochem. Soc.*, **2011**, *158*, A250.

15. D. Rangappa, K. Sone, Y. Zhou, T. Kudo and I. Honma. *J. Mater. Chem.*, **2011**, *21*, 15813.

16. M. Pivko, M. Bele, E. Tchernychova, N. Z. Logar, R. Dominko and M. Gaberscek. *Chem. Mater.*, **2012**, *24*, 1041–1047.

17. N. Ravet, J. B. Goodenough, S. Besner, M. Simoneau, P. Hovington and M. Armand. *Abstr. 127, Electrochem. Soc. Electrochem. Soc. Japan Meet. Abstr. Vol. 99–2, Honolulu, Hawaii, Oct 17–22*, **1999**, *99–2*, .

18. H. Huang, S.-C. Yin and L. F. Nazar. *Electrochem. Solid-State Lett.*, **2001**, *4*, A170.

19. A. Yamada, S. C. Chung and K. Hinokuma. *J. Electrochem. Soc.*, **2001**, *148*, A224.

20. J. Chen and M. S. Whittingham. *Electrochem. commun.*, **2006**, *8*, 855–858.

21. Z. Chen and J. R. Dahn. *J. Electrochem. Soc.*, **2002**, *149*, A1184.

22. S. Franger, F. Le Cras, C. Bourbon and H. Rouault. *Electrochem. Solid-State Lett.*, **2002**, *5*, A231.

23. B. L. Cushing and J. B. Goodenough. *Solid State Sciences*, **2002**, *4*, 1487–1493.

24. R. Dominko, M. Bele, M. Gaberscek, M. Remskar, D. Hanzel, S. Pejovnik and J. Jamnik. *J. Electrochem. Soc.*, **2005**, *152*, A607.

25. R. Dominko, D. E. Conte, D. Hanzel, M. Gaberscek and J. Jamnik. *J. Power Sources*, **2008**, *178*, 842–847.

26. M. Küzma, R. Dominko, A. Meden, D. Makovec, M. Bele, J. Jamnik and M. Gaberšček. *J. Power Sources*, **2009**, *189*, 81–88.

27. Z. L. Gong, Y. X. Li, G. N. He, J. Li and Y. Yang. *Electrochem. Solid-State Lett.*, **2008**, *11*, A60.

28. R. Dominko, M. Bele, J. M. Goupil, M. Gaberscek, D. Hanzel, I. Arcon and J. Jamnik. *Chem. Mater.*, **2007**, *19*, 2960–2969.

29. J. Moskon, M. Pivko, I. Jerman, E. Tchernychova, N. Z. Logar, M. Zorko, V. S. Selih, R. Dominko and M. Gaberscek. *J. Power Sources*, **2016**, *303*, 97–108.

30. D. Wang, C. Ouyang, T. Dre´zen, I. Exnar, A. Kay, N.-H. Kwon, P. Gouerec, J. H. Miners, M. Wang and M. Gra¨tzel. *J. Electrochem. Soc.*, **2010**, *157*, A225.

31. T. Shiratsuchi, S. Okada, T. Doi and J. I. Yamaki. *Electrochim. Acta*, **2009**, *54*, 3145–3151.

32. H. Yoo, M. Jo, B. S. Jin, H. S. Kim and J. Cho. *Adv. Energy Mater.*, **2011**, *1*, 347–351.

33. V. A. Streltsov, E. L. Belokoneva, V. G. Tsirelson and N. K. Hansen. *Acta Crystallogr.*, **1993**, *49*, 147–153.

34. M. S. Whittingham. *Chem. Rev.*, **2014**, *114*, 11414–11443.

35. J. Syzdek, M. Marcinek and R. Kostecki. *J. Power Sources*, **2014**, *245*, 739–744.

36. R. Amin, P. Balaya and J. Maier. *Electrochem. Solid-State Lett.*, **2007**, *10*, A13.

37. M. Köhler, F. Berkemeier, T. Gallasch and G. Schmitz. *J. Power Sources*, **2013**, *236*, 61–67.

38. P. P. Prosini, M. Lisi, D. Zane and M. Pasquali. *Solid State Ionics*, **2002**, *148*, 45–51.

39. H. C. Dinh, S. Il Mho, Y. Kang and I. H. Yeo. *J. Power Sources*, **2013**, *244*, 189–195.

40. D. Fujimoto, N. Kuwata, Y. Matsuda, J. Kawamura and F. Kang. *Thin Solid Films*, **2015**, *579*, 81–88.

41. J. N. Reimers and J. R. Dahn. *Journal of The Electrochemical Society*, **1992**, *139*, 2091.

42. W. Dreyer, J. Jamnik, C. Guhlke, R. Huth, J. Moskon and M. Gaberscek. *Nat. Mater.*, **2010**, *9*, 448–453.

43. C. Fongy, S. Jouanneau, D. Guyomard, J. C. Badot and B. Lestriez. *J. Electrochem. Soc.*, **2010**, *157*, A1347.

44. C. Fongy, A.-C. Gaillot, S. Jouanneau, D. Guyomard and B. Lestriez. *J. Electrochem. Soc.*, **2010**, *157*, A885.

45. D. P. Singh, F. M. Mulder and M. Wagemaker. *Electrochem. commun.*, **2013**, *35*, 124–127.

46. D. P. Singh, F. M. Mulder, A. M. Abdelkader and M. Wagemaker. *Adv. Energy Mater.*, **2013**, *3*, 572–578.

47. M. Gaberscek, R. Dominko and J. Jamnik. *Electrochem. commun.*, **2007**, *9*, 2778–2783.

48. M. Gaberscek, M. Küzma and J. Jamnik. *Phys. Chem. Chem. Phys.*, **2007**, *9*, 1815–1820.

49. Y. Oumellal, N. Delpuech, D. Mazouzi, N. Dupré, J. Gaubicher, P. Moreau, P. Soudan, B. Lestriez and D. Guyomard. *J. Mater. Chem.*, **2011**, *21*, 6201.

50. W. C. Chueh, F. El Gabaly, J. D. Sugar, N. C. Bartelt, A. H. McDaniel, K. R. Fenton, K. R. Zavadil, T. Tyliszczak, W. Lai and K. F. McCarty. *Nano Lett.*, **2013**, *13*, 866–872.

51. Y. Li, F. El Gabaly, T. R. Ferguson, R. B. Smith, N. C. Bartelt, J. D. Sugar, K. R. Fenton, D. a Cogswell, a L. D. Kilcoyne, T. Tyliszczak, M. Z. Bazant and W. C. Chueh. *Nat. Mater.*, **2014**, *13*, 1149–1156.

52. C. Delmas, M. Maccario, L. Croguennec, F. Le Cras and F. Weill. *Nat. Mater.*, **2008**, *7*, 665–671.

53. G. Brunetti, D. Robert, P. Bayle-Guillemaud, J. L. Ouvi, E. F. Rauch, J. F. Martin, J. F. Colin, F. Bertin and C. Cayron. *Chem. Mater.*, **2011**, *23*, 4515–4524.

54. J. D. Sugar, F. El Gabaly, W. C. Chueh, K. R. Fenton, T. Tyliszczak, P. G. Kotula and N. C. Bartelt. *J. Power Sources*, **2014**, *246*, 512–521.

55. T. R. Ferguson and M. Z. Bazant. *J. Electrochem. Soc.*, **2012**, *159*, A1967–A1985.

56. R. Malik, A. Abdellahi and G. Ceder. *J. Electrochem. Soc.*, **2013**, *160*, A3179–A3197.

57. B. Orvananos, R. Malik, H. C. Yu, A. Abdellahi, C. P. Grey, G. Ceder and K. Thornton. *Electrochim. Acta*, **2014**, *137*, 245–257.

58. X. Zhang, M. Van Hulzen, D. P. Singh, A. Brownrigg, J. P. Wright, N. H. Van Dijk and M. Wagemaker. *Nano Lett.*, **2014**, *14*, 2279–2285.

59. H. Liu, F. C. Strobridge, O. J. Borkiewicz, K. M. Wiaderek, K. W. Chapman, P. J. Chupas and C. P. Grey. *Science (80-.).*, **2014**, *344*, 1451–1452.

Povzetek

Osnovne elektrokemijske karakteristike baterijskega materiala na osnovi $LiMnPO_4$ primerjamo s karakteristikami precej bolj raziskanega materiala na osnovi spojine $LiFePO_4$ z olivinsko strukturo ter prav tako dobro znanega materiala na osnovi $LiCoO_2$. Na podlagi obsežnejših kronopotenciometričnih (galvanostatskih) meritev primerjamo energijsko učinkovitost in prenapetost elektrod, narejenih iz omenjenih materialov. V ta namen za odčitavanje celotne prenapetosti, η_{total}, uvedemo in utemeljimo tako imenovani "kriterij točke prevoja". V nadaljevanju pokažemo, da lahko v splošnem tokovno-napetostno karakteristiko insercijskih elektrod predstavimo z enostavnim parametrom – celotno upornostjo elektrode, R_{total}. Medtem ko je tokovno-napetostna karakteristika elektrode na osnovi $LiCoO_2$ približno linearna, pa pride v primeru $LiFePO_4$, in še bolj $LiMnPO_4$, do znatnega odstopanja od linearnosti. Pojav razložimo s sklicevanjem na najnovejše ugotovitve o pojavih fazne transformacije v omenjenih baterijskih sistemih.